

Impact of Massive Black Hole Binaries Source Confusion on Uncertainties of Parameters Estimation in Space-based Gravitational Wave Detection for the TaiJi Mission*

Qing Diao¹, Hongxin Wang², He Wang¹, Jun Nian¹, Peng Xu^{3,4,5,*}, Minghui Du^{3,*}

¹*International Centre for Theoretical Physics Asia-Pacific,*

University of Chinese Academy of Sciences, 100190 Beijing, China

²*School of Software, Northwestern Polytechnical University, Xian 710072, China*

³*Taiji Laboratory for Gravitational Wave Universe (Beijing/Hangzhou),*

University of Chinese Academy of Sciences, 100049 Beijing, China

⁴*Center for Gravitational Wave Experiment, National Microgravity Laboratory, Institute of Mechanics, Chinese Academy of Sciences, Beijing 100190, China*

⁵*Key Laboratory of Gravitational Wave Precision Measurement of Zhejiang Province,*

Hangzhou Institute for Advanced Study, University of Chinese Academy of Sciences, Hangzhou 310024, China

We systematically investigate the impact of source confusion on parameter estimation for massive black hole binaries (MBHBs) in the context of the Taiji space-based gravitational wave mission. Three representative MBHB population models—PopIII, Q3d, and Q3nod—are considered. By performing high-precision numerical simulations and employing both the Fisher information matrix and Markov chain Monte Carlo (MCMC) techniques, we quantitatively assess the uncertainties in parameter estimation. Source confusion primarily arises from overlapping time-frequency tracks of multiple signals. We find that when the relative difference in detector-frame chirp masses between two signals is extremely small ($\Delta\mathcal{M}_z/\mathcal{M}_z < 0.2\%$), the uncertainty in parameter estimation increases significantly. However, this degradation can be substantially mitigated by incorporating higher-order modes into the waveform model. Furthermore, using full Bayesian inference, we demonstrate the clear advantage of higher-order modes in reducing systematic biases in parameter recovery. These results provide important guidance for future data analysis strategies in space-based gravitational wave observations.

I. INTRODUCTION

The detection of gravitational waves (GWs) from binary black hole mergers by ground-based observatories such as LIGO has ushered in the era of gravitational wave astronomy, opening new avenues for exploring the cosmos. Unlike terrestrial detectors, space-based observatories including TaiJi, LISA, and TianQin will operate in the millihertz frequency band, enabling the detection of gravitational waves from massive black hole binaries (MBHBs) and other astrophysically rich sources. The anticipated event rates for MBHB mergers span from a few to several hundred per year, potentially resulting in significant source confusion due to overlapping signals within detector data streams. Such confusion poses critical challenges for the accurate estimation of astrophysical parameters, affecting both single-parameter estimation (SPE) and joint-parameter estimation (JPE).

The landmark detection of gravitational waves by the Laser Interferometer Gravitational-Wave Observatory (LIGO) from stellar-mass black hole mergers has inaugurated gravitational wave astronomy, fundamentally enhancing our capability to explore cosmic phenomena [1-2]. Ground-based detectors, however, encounter intrinsic limitations due to seismic and gravitational gradient noise, constraining their sensitivity predominantly

to frequencies above tens of hertz. Extending gravitational wave detection capabilities into the low-frequency range (from to 1 Hz) necessitates space-based observatories, which provide unparalleled sensitivity and the ability to detect diverse astrophysical sources, such as MBHBs, stellar-mass black hole binaries, white dwarf binaries, and extreme mass-ratio inspirals (EMRIs) [3].

Proposed space-based gravitational wave detectors, including the Laser Interferometer Space Antenna (LISA), TaiJi, and TianQin, promise to open new observational windows onto the universe. Specifically, the TaiJi mission, initiated by the Chinese Academy of Sciences, will employ a triangular satellite formation with arm lengths of km in heliocentric Earth-like orbits [5]. Gravitational wave signals will be inferred from optical path differences measured through laser interferometry. Extracting these signals from noisy data streams demands highly accurate waveform templates, precise detector response modeling, advanced noise-reduction methods, and sophisticated parameter estimation algorithms grounded in Bayesian statistics.

Nevertheless, increasing detector sensitivity is expected to yield numerous overlapping gravitational wave signals, complicating the identification and analysis of individual events [7]. Overlapping signals induce significant biases in parameter estimation, complicating both SPE and JPE approaches. While JPE simultaneously analyzes multiple signals, it requires substantial computational resources. Conversely, SPE, although computationally more efficient, may exhibit large systematic bi-

* duminghui@imech.ac.cn
xupeng@imech.ac.cn

ases under substantial confusion. Consequently, understanding SPE behavior under conditions of confusion is crucial prior to adopting more computationally intensive JPE analyses [13].

MBHBs, predicted to fall within the mass range of to solar masses, constitute some of the most promising targets for space-based gravitational wave astronomy [14]. Current understanding of this astrophysical population remains incomplete regarding mass distribution, spin characteristics, formation pathways, and evolutionary trajectories. Observations of gravitational waves emitted by MBHB mergers, particularly those with high signal-to-noise ratios, will significantly enhance our knowledge of massive black holes and their interactions with host galaxies.

Given the variation in predicted MBHB merger rates across population models (e.g., approximately 174.7 events per year for Pop III and about 122.44 per year for Q3nod [15]), assessing source confusion and its implications for parameter estimation is essential. Previous source confusion studies have primarily concentrated on ground-based detectors, with relatively sparse consideration for space-based observatories. Consequently, this study systematically explores MBHB source confusion for multiple population models, evaluating overlap statistics and distributions within the TaiJi sensitivity band and their implications for parameter estimation uncertainties.

II. THEORETICAL FRAMEWORK AND SIMULATION SETUP

A. MBHB Population Models

Massive black hole binary (MBHB) populations emerge from distinct seeding mechanisms, each with unique mass distributions observable by gravitational-wave detectors. Three primary models—Pop III, Q3d, and Q3nod—highlight these differences.

The Pop III model assumes MBH seeds from Population III stars, forming "light seeds" ($10^2, M_\odot$) at high redshifts. Delays from dynamical friction produce a lower-mass binary distribution (10^4 – $10^6, M_\odot$), challenging gravitational-wave detection.

In the heavy-seed scenario (Q3d), direct collapse forms massive seeds ($10^5, M_\odot$). Merger delays lower event rates but yield massive binaries (10^5 – $10^7, M_\odot$) detectable by gravitational-wave observatories.

Q3nod mirrors Q3d seed formation but excludes delays, significantly increasing merger rates while retaining massive binaries. This scenario broadens the mass spectrum and elevates merger frequencies.

Distinguishing among these mass distributions through gravitational-wave observations provides critical insights into black hole formation and galaxy evolution.

B. The Prevalence of source confusion

In this study, we adopt the numerical simulation approach proposed in Ref.[16], which combines observationally inferred local merger rates with MBHB population models. The delay between the formation of black hole seeds and their eventual coalescence is explicitly incorporated. Under different assumptions for the local merger rate, we compute the total number of merger events per year (N_{MBHB}) and the mean time interval between successive events ($\langle \Delta t_c \rangle$, in days). The results are summarized in Table I, which demonstrates a strong sensitivity of the event statistics to the assumed merger rate. By adjusting the event rate assumptions, this methodology can be flexibly applied to various detector configurations and MBHB population scenarios.

TABLE I. Total number of MBHB merger events per year (N_{MBHB}) and mean time interval between consecutive events ($\langle \Delta t_c \rangle$, in days) under different assumptions of local merger rate. Delay-time effects are included in all cases.

Rate [$\text{Gpc}^{-3} \text{ yr}^{-1}$]	N_{MBHB}	$\langle \Delta t_c \rangle$ [days]
0.01	13	13.3
0.05	71	2.5
0.07	100	1.8
0.5	723	0.3
1.0	1444	0.1
5.0	7238	0.03

It is important to emphasize that source confusion arises not merely from overlap in either time or frequency, but rather from simultaneous overlap in both domains. To explicitly characterize the source confusion statistics and their time-frequency distributions across different MBHB populations, we conduct detailed numerical simulations for the PopIII, Q3d, and Q3nod models. Specifically, we use the `BBHx` package with the `IMRPhenomHM` waveform model, incorporating numerical orbital evolution and second-generation time-delay interferometry (TDI) to model the detector response under realistic mission configurations.

TABLE II. List of source parameters used in the simulations, along with their corresponding symbols and physical units.

Parameter	Symbol	Unit
Detector-frame chirp mass	\mathcal{M}_z	M_\odot
Mass ratio	q	-
Primary spin (aligned)	a_{1z}	-
Secondary spin (aligned)	a_{2z}	-
Coalescence time	t_c	day
Coalescence phase	Φ_c	rad
Luminosity distance	D_L	Mpc
Inclination angle	ι	rad
Ecliptic longitude	λ	rad
Ecliptic latitude	β	rad
Polarization angle	ψ	rad

The simulated source parameters include intrinsic and

extrinsic quantities relevant to space-based gravitational wave detection. These parameters and their associated symbols and units are summarized in Table II. The simulations assume a local merger rate of $0.07 \text{ Gpc}^{-3} \text{ yr}^{-1}$, yielding approximately 50 signals within a half-year observation window. To mitigate edge effects caused by data truncation, the coalescence time of the target signal is placed at the center of the observation window.

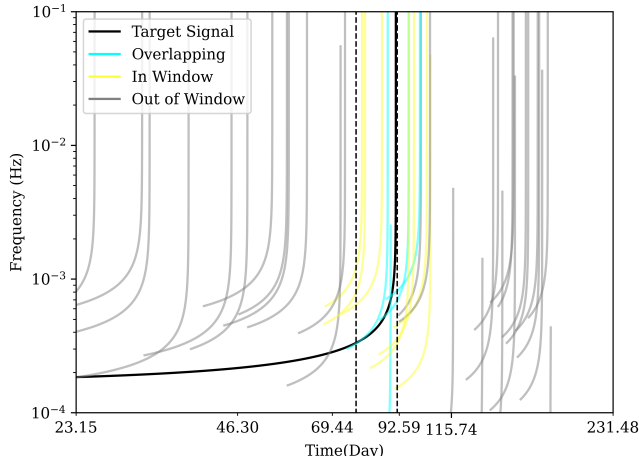


FIG. 1. Time-frequency map of a representative PopIII simulation. Yellow traces denote all signals overlapping with the target signal (black) in the time domain; blue traces indicate signals with simultaneous overlap in both time and frequency domains.

Figure 1 shows a representative example from the PopIII population. Although multiple signals (yellow) overlap with the target signal (black) in the time domain, only a small subset (blue) exhibit simultaneous overlap in both time and frequency. To ensure statistical robustness, the number of simulations for each population model is determined based on the central limit theorem. For the PopIII model, 1285 simulations were performed, yielding a mean overlap count of 2.092 (target error margin $\epsilon = 0.1$, confidence level 98%); for the Q3d model, 511 simulations resulted in an average of 0.1565 overlaps ($\epsilon = 0.05$, 98% confidence); and for the Q3nod model, 775 simulations gave an average of 0.174 overlaps ($\epsilon = 0.05$, 98% confidence). These results indicate that the occurrence of source confusion among MBHBs is relatively rare and is predominantly limited to pairwise interactions between signals.

C. Parameter Uncertainty Quantification

To evaluate the impact of source confusion on the parameter estimation of massive black hole binaries (MBHBs), we employ two complementary approaches: the Fisher information matrix and Markov Chain Monte Carlo (MCMC) sampling. The Fisher matrix method approximates the posterior distribution as Gaussian in

the high signal-to-noise ratio (SNR) regime and provides a rapid estimate of parameter variances and covariances. It is widely used for forecasting parameter uncertainties in gravitational wave missions.

We first compute the uncertainty $\Delta\theta^i$ of the i -th parameter for an isolated target signal. We then introduce a second signal that partially overlaps with the target and compute the corresponding uncertainty under confusion, denoted $\Delta\Theta^i$. The ratio of uncertainties is defined as: $\rho = \Delta\Theta^i / \Delta\theta^i$, where both $\Delta\theta^i$ and $\Delta\Theta^i$ are derived from the respective Fisher information matrices. By analytically identifying the key parameters that influence ρ —such as the time separation between coalescences, the relative difference in chirp masses, and the characteristic frequency at overlap—we systematically investigate how variations in these quantities affect the degradation of parameter precision. In addition, we compare scenarios with and without the inclusion of higher-order modes, revealing differences in source resolvability across different population models.

To assess the potential bias introduced by source confusion in realistic data analysis settings, we further apply full Bayesian inference using the MCMC method in representative cases with significant degradation. The Markov Chain Monte Carlo technique is a class of sampling algorithms rooted in Bayesian statistics and is commonly employed for parameter estimation in the presence of complex posterior distributions. In gravitational wave data analysis, MCMC has become a central tool, particularly well-suited for high-dimensional parameter spaces where posterior distributions are non-Gaussian or analytically intractable.

The Fisher matrix and MCMC methods offer complementary insights: while the Fisher matrix provides fast uncertainty estimates under the high-SNR assumption, MCMC enables full reconstruction of the posterior landscape, capturing effects such as non-Gaussianity and parameter degeneracies. Consequently, Fisher-based forecasts are often used in early-stage mission design and sensitivity studies, whereas MCMC is applied for final validation and precise inference in actual data analysis.

1. Fisher Matrix Methodology

In space-based gravitational wave detectors such as LISA, multiple signals from compact binaries can overlap in time-frequency space, leading to source confusion. This phenomenon occurs when the time-frequency tracks of signals cross, resulting in nonzero cross-correlations that impact parameter estimation.

The total data stream consists of stationary, Gaussian noise $Noise(t)$ and multiple signals $h_n(t; \theta_n)$:

$$s(t) = \sum_{n=1}^N h_n(t; \theta_n) + Noise(t), \quad (1)$$

where θ_n represents the set of parameters for each indi-

vidual signal.

The likelihood function for this model is given by:

$$p(s|\Theta) \propto \exp \left[-\frac{1}{2} (s - H(\Theta)|s - H(\Theta)) \right], \quad (2)$$

where $\Theta = (\theta_1, \theta_2, \dots, \theta_N)$ is the full parameter set, and the noise-weighted inner product is defined as:

$$(h|g) = 4 \operatorname{Re} \int_0^\infty \frac{\tilde{h}(f)\tilde{g}^*(f)}{S_n(f)} df. \quad (3)$$

Here, $S_n(f)$ is the one-sided noise power spectral density, and tildes denote Fourier transforms.

The Fisher matrix, which provides an approximation for parameter uncertainties, is given by:

$$\Gamma_{ij} = \left(\frac{\partial H}{\partial \theta^i} \middle| \frac{\partial H}{\partial \theta^j} \right). \quad (4)$$

The covariance matrix, which determines the parameter uncertainties, is obtained by inverting the composite Fisher matrix:

$$\Sigma = \Gamma^{-1}. \quad (5)$$

The parameter uncertainty ratio is defined as:

$$\rho = \frac{\Delta \theta^i}{\Delta \theta^i} = \sqrt{\frac{(\Gamma^{-1})_{ii}}{(\gamma^{-1})_{ii}}}, \quad (6)$$

where γ is the Fisher matrix for a single signal, and Γ is the Fisher matrix including source confusion effects.

The composite Fisher matrix defined in Eq. (4) consists of individual Fisher matrices for each signal along the diagonal and off-diagonal cross-terms due to overlapping signals:

$$\Gamma = \begin{bmatrix} \gamma_{ij}^{(1)} & C_{ij}^{(12)} \\ C_{ij}^{(21)} & \gamma_{ij}^{(2)} \end{bmatrix}. \quad (7)$$

The off-diagonal terms, which account for the coupling between overlapping signals, are given by:

$$C_{ij}^{(12)} = \left(\frac{\partial h_1}{\partial \theta^i} \middle| \frac{\partial h_2}{\partial \theta^j} \right), \quad (8)$$

and influence the overall parameter estimation precision.

To assess the impact of two signals on the overall parameter uncertainties, the cross-term integral is considered:

$$I = (h'_1|h'_2) = 4 \Re \int \frac{h'_1(f) h'_2{}^*(f)}{S_n(f)} df, \quad (9)$$

where $h'_i(f)$ denotes the derivative of the waveform with respect to a given parameter, and $S_n(f)$ is the noise power spectral density.

To overcome the difficulties associated with the high-frequency oscillations in the integral, the stationary

phase approximation (SPA) is adopted. In this approach, one locates the stationary point f_F of the phase difference $\Delta\Psi(f)$ by imposing

$$\left. \frac{d\Delta\Psi}{df} \right|_{f=f_F} = 0. \quad (10)$$

Under the SPA, the cross-term integral is approximately given by the key Equation (E7)(see Ref. [16]):

$$I \approx 4 \Re \left[\exp \left\{ i\Delta\Psi(f_F) + i\frac{\pi}{4} \operatorname{sign} \left(d^2\Delta\Psi/df^2(f_F) \right) \right\} \times \frac{|A(f_F)|}{S_n(f)} \sqrt{\frac{2\pi}{|d^2\Delta\Psi/df^2(f_F)|}} \right]. \quad (11)$$

The Fisher stationary point f_F is not the same as the frequency f_{ov} at which the time-frequency tracks cross, i.e.,

$$\left. \frac{d(\Phi_1 - \Phi_2)}{df} \right|_{f=f_{ov}} = 0. \quad (12)$$

In practice, however, their difference is on the order of $O(10^{-2})$ Hz. Although Eq. (11) is evaluated self-consistently using f_F , in the main text the distinction between f_F and f_{ov} is largely dropped.

Equation (11) indicates that the contribution of the cross-term is primarily determined by:

1. the frequency at which the time-frequency tracks overlap f_{ov} ,
2. The amplitude $|A(f_{ov})|$ of the signal at f_{ov} ;
3. The second derivative of the phase $d^2\Delta\Psi/df^2(f_{ov})$;
4. The phase offset $\Delta\Psi(f_{ov})$ at f_{ov} .

Thus, this expression provides the theoretical basis for quantitatively describing how the cross-terms between two overlapping signals contribute to the composite Fisher matrix, and thereby, for assessing the effect of source confusion on parameter uncertainty when signals overlap in both time and frequency.

III. IMPACT OF SOURCE CONFUSION ANALYSIS VIA FISHER MATRIX

Based on the analysis in Sec. II.B, source confusion in space-based gravitational wave observations of MBHBs typically involves only two overlapping signals. Therefore, our study focuses on confusion arising between two sources. As shown in Eq. (11) of Sec. II.C.1, the amplitude at the overlap frequency, $A(f_{ov})$, is primarily determined by the detector-frame chirp mass \mathcal{M}_z , while the slope of the time-frequency trajectory depends on both

\mathcal{M}_z and the overlap frequency f_{ov} . As f_{ov} increases, the trajectory slope also increases.

In this work, we systematically investigate the impact of three key variables on parameter uncertainty induced by source confusion: the overlap frequency f_{ov} , the phase difference at overlap $\Delta\Phi(f_{\text{ov}}) = \Phi_{c1} - \Phi_{c2}$, and the chirp mass difference $\Delta\mathcal{M}_z = |\mathcal{M}_{z1} - \mathcal{M}_{z2}|$. We further explore a range of chirp mass scales accessible to space-based detectors (10^4 – $10^7 M_\odot$), and compare results with and without higher-order modes in waveform modeling.

The parameter sets used for the two simulated signals are as follows:

- **parameters1:** $\mathcal{M}_z = 10^4$, $q = 0.87$, $a_{1z} = 0.90$, $a_{2z} = 0.92$, $t_c = 30.0$, $\Phi_c = 0.5$, $D_L = 30,200$, $\iota = 0.88$, $\lambda = 3.35$, $\beta = 0.12$, $\psi = 1.56$;
- **parameters2:** $\mathcal{M}_z = 10^4$, $q = 0.87$, $a_{1z} = 0.899$, $a_{2z} = 0.921$, $t_c = 30.0$, $\Phi_c = 0.58$, $D_L = 30,210$, $\iota = 0.60$, $\lambda = 3.338$, $\beta = 0.11$, $\psi = 1.68$.

The units for all parameters listed below are given in Table II. Unless otherwise specified, we vary only three parameters between the two signals: the chirp mass, coalescence phase, and coalescence time. By tuning the latter two, we control the relative position of the signals in the time-frequency domain, thereby adjusting f_{ov} and $\Delta\Phi$.

A. Effects of Chirp Mass Magnitude and Higher-Order Modes

According to previous studies, parameter uncertainties increase significantly when two signals exhibit similar time-frequency trajectories, which is largely determined by their detector-frame chirp masses. Signals with comparable \mathcal{M}_z values have overlapping trajectories over broader frequency ranges, enhancing cross-correlation and increasing confusion. Theoretically, higher-order modes possess distinct time-frequency evolution and can therefore help to resolve overlapping sources.

Figure 2 shows the parameter uncertainty ratio ρ for the case $\Delta\mathcal{M}_z = 0$, under different chirp mass scales. Dashed lines correspond to waveforms with only the dominant (2,2) mode, while solid lines include higher-order modes. Since signals with different \mathcal{M}_z values span different frequency ranges, the chosen overlap frequency f_{ov} decreases with increasing \mathcal{M}_z , while the phase difference at overlap is fixed at $\Delta\Phi(f_{\text{ov}}) = 0$.

Overall, we observe that ρ increases significantly with chirp mass, indicating stronger parameter degradation in high-mass systems. However, the inclusion of higher-order modes consistently mitigates this effect. For most parameters—except luminosity distance D_L and inclination angle ι —the increase in uncertainty due to source confusion remains within an order of magnitude of $\mathcal{O}(10^1)$ compared to the isolated case. While D_L and ι exhibit larger increases, their uncertainty remains below

$\mathcal{O}(10^3)$ of the non-confused case, where typical uncertainties are $\sim \mathcal{O}(10^{-9})$ and $\sim \mathcal{O}(10^{-4})$, respectively. These findings indicate that source confusion significantly affects parameter estimation only when the chirp masses are nearly identical, and that higher-order modes offer a robust mitigation strategy.

B. Parameter Uncertainty Variation and the Ratio ρ with Overlapping Signals

We consider two representative chirp mass scales, $\mathcal{M}_z = 10^5$ and $\mathcal{M}_z = 10^6$, and investigate the impact of the chirp mass difference $\Delta\mathcal{M}_z$ on the parameter uncertainty ratio ρ , both with and without higher-order modes. Results are shown in Fig. 3. Additional results for $\mathcal{M}_z = 10^4$ and 10^7 are provided in Appendix A. As clearly shown, the most significant increase in parameter uncertainty due to source confusion occurs when $\Delta\mathcal{M}_z \rightarrow 0$, consistent with existing literature. Moreover, the uncertainty mitigation effect of higher-order modes becomes more pronounced as \mathcal{M}_z increases.

Further analysis reveals that within the chirp mass range most relevant to the Taiji mission (10^4 , 10^5 , 10^6 , and $10^7 M_\odot$), the parameter uncertainty ratio $\rho(-1)$ only increases beyond $\mathcal{O}(10^1)$ when the relative chirp mass difference $\Delta\mathcal{M}_z/\mathcal{M}_z$ falls below 0.2%. Even in this extreme case, the uncertainty increase remains below an order of $\mathcal{O}(10^1)$ compared to the non-confused baseline. For lower chirp masses (10^4 – $10^5 M_\odot$), the increase is even milder and stays within $\mathcal{O}(10^0)$. Based on numerical simulations of the PopIII, Q3d, and Q3nod population models—excluding MBHBs outside the Taiji sensitivity band—we find that the fraction of overlapping events with $\Delta\mathcal{M}_z < 0.2\%$ (relative to the smaller mass in the pair) is 0.14% (0.08%, 0.12%) for the three models, respectively.

Figure 4 further illustrates the dependence of $\rho(-1)$ on the overlap frequency f_{ov} for different \mathcal{M}_z values. Due to differences in the frequency coverage of each mass scale, the range of f_{ov} varies accordingly. For lower-mass systems ($\mathcal{M}_z = 10^4$ and 10^5), $\rho - 1$ remains nearly constant as f_{ov} increases, showing little fluctuation. The uncertainties for spin parameters a_{1z} and a_{2z} nearly coincide. In contrast, for higher-mass systems ($\mathcal{M}_z = 10^6$ and 10^7), and particularly when higher-order modes are included, the uncertainty ratio shows more pronounced fluctuations as f_{ov} varies, with sharp increases observed near certain frequencies. In the extreme case of $\mathcal{M}_z = 10^7$, using only the (2,2) mode can result in large estimation errors. Overall, the inclusion of higher-order modes significantly suppresses the growth of $\rho - 1$ due to source confusion. Even in the worst-case scenario of $\Delta\mathcal{M}_z = 0$, the resulting $\rho - 1$ remains within $\mathcal{O}(10^1)$, and does not exceed $\mathcal{O}(10^2)$.

As shown in Fig. 5, the variation of $\rho - 1$ with $\Delta\Phi \in [0, 2\pi]$ exhibits a nearly symmetric mirror pattern between the intervals $[0, \pi]$ and $[\pi, 2\pi]$, though numerical

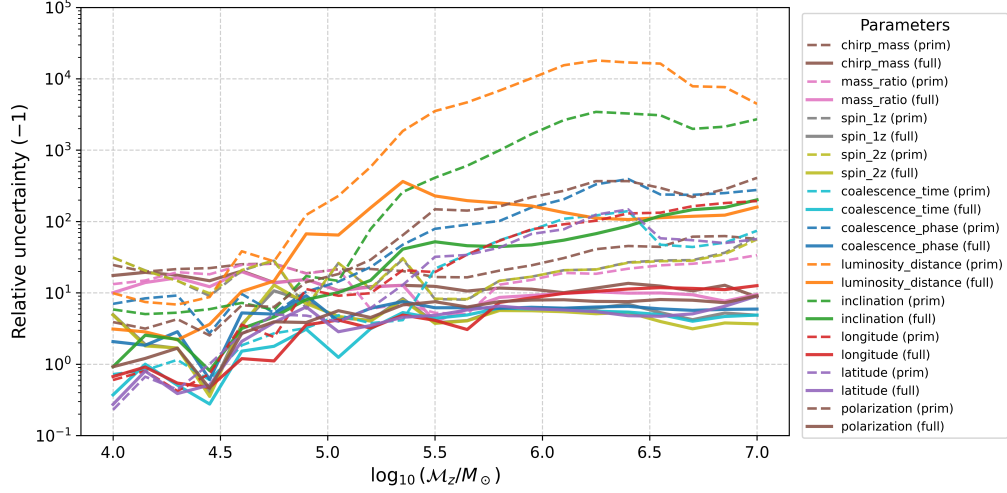


FIG. 2. Parameter uncertainty ratio $\rho(-1)$ as a function of chirp mass scale for the case $\Delta\mathcal{M}_z = 0$. Solid lines represent waveforms including higher-order modes; dashed lines show results for the dominant (2,2) mode only. The phase difference at overlap is fixed ($\Delta\phi = 0$), and the relative overlap location in the time-frequency trajectory is kept constant.

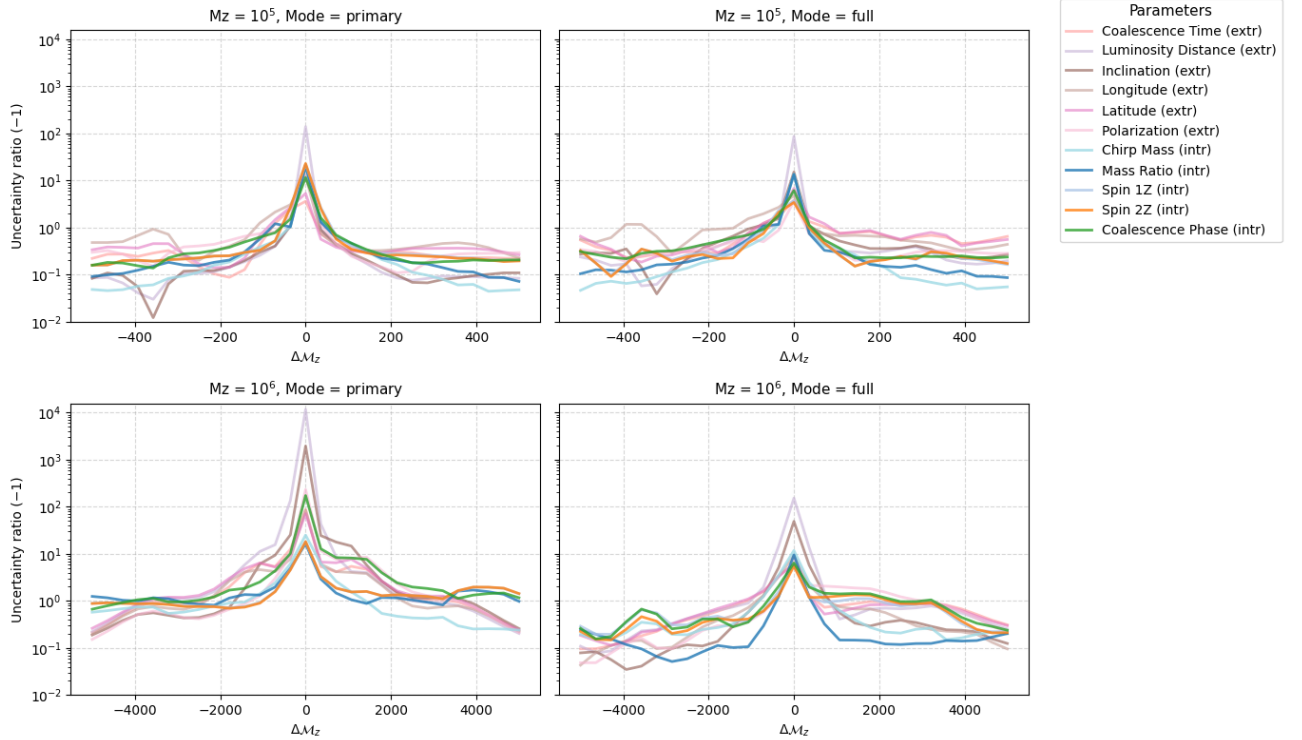


FIG. 3. Parameter uncertainty ratio $\rho(-1)$ as a function of chirp mass difference $\Delta\mathcal{M}_z$ for $\mathcal{M}_z = 10^5$ (top) and $\mathcal{M}_z = 10^6$ (bottom). Left panels consider only the dominant (2,2) mode, while right panels include higher-order modes. The range of $\Delta\mathcal{M}_z$ spans 1% of the respective \mathcal{M}_z , with $\Delta\Phi = 0$ and a fixed relative position in the time-frequency trajectory.

differences are present. Generally, $\rho - 1$ reaches a local maximum at $\Delta\Phi = 0$, decreases to a local minimum at $\Delta\Phi = \pi$, and then increases again, indicating a periodic modulation of time-frequency overlap due to phase difference. The uncertainties in a_{1z} and a_{2z} remain nearly identical throughout, suggesting that source confusion

impacts them in a highly similar manner.

Although this section focuses on the extreme case of $\Delta\mathcal{M}_z = 0$, the results show that even under such conditions, the inclusion of higher-order modes keeps $\rho - 1$ mostly within $\mathcal{O}(10^1)$ and always below $\mathcal{O}(10^2)$. The large fluctuations observed in the $\mathcal{M}_z = 10^7$ case may

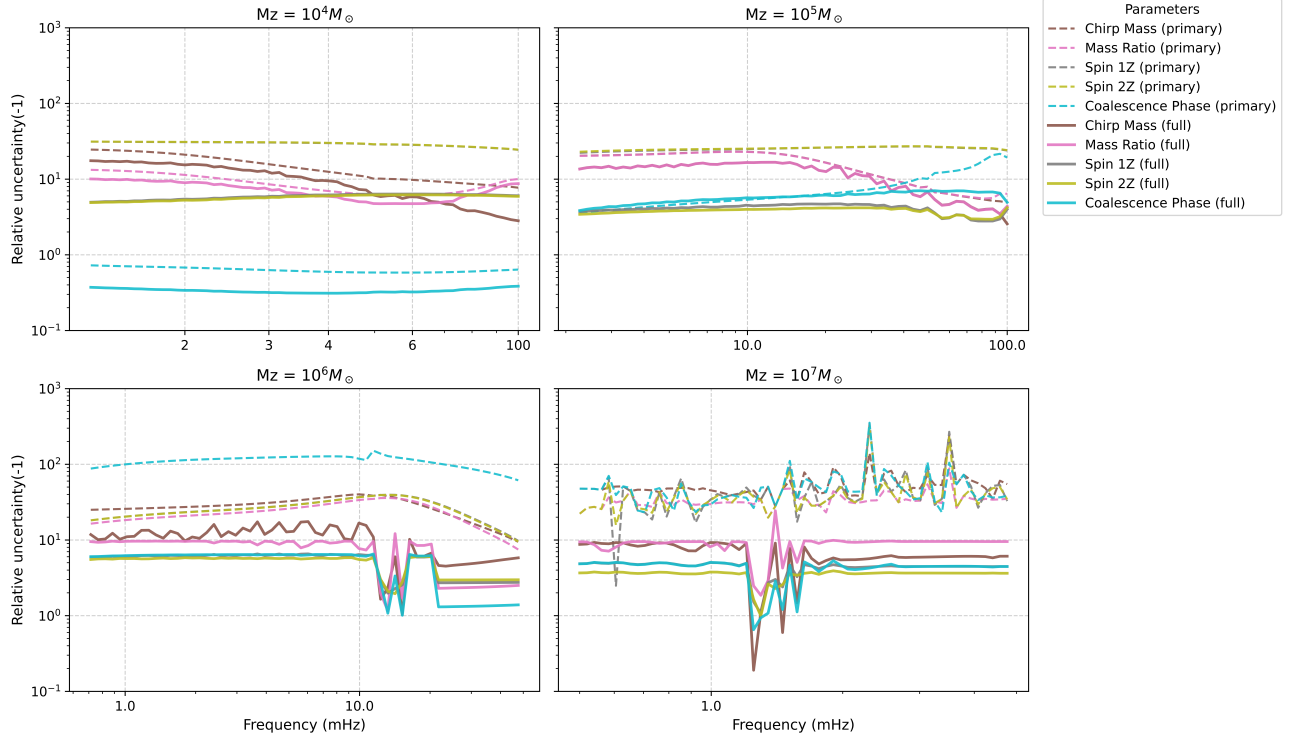


FIG. 4. Variation of the parameter uncertainty ratio $\rho(-1)$ with increasing overlap frequency f_{ov} for different chirp mass scales. Only intrinsic parameters are shown. Dashed lines represent waveforms with only the dominant (2,2) mode; solid lines include higher-order modes. All cases use $\Delta\mathcal{M}_z = 0$ and $\Delta\Phi = 0$.

be attributed to the narrower time-frequency evolution range of high-mass systems, which enhances signal overlap and cross-correlation effects at certain phase differences. This sensitivity highlights the crucial role of higher-order modes in accurate modeling and parameter inference.

C. Full Bayesian Inference with Overlapping MBHB Signals

Based on the previous statistical analysis, we select a representative pair of MBHB signals exhibiting strong source confusion for full Bayesian inference using MCMC sampling. The parameter sets of the two signals are as follows:

- **parameters1:** $\mathcal{M}_z = 10^5$, $q = 0.52$, $a_{1z} = 0.90$, $a_{2z} = 0.92$, $t_c = 30.0$, $\Phi_c = 0.5$, $D_L = 30,200$, $\iota = 0.82$, $\lambda = 3.35$, $\beta = 0.045$, $\psi = 1.56$;
- **parameters2:** $\mathcal{M}_z = 10^5$, $q = 0.50$, $a_{1z} = 0.90$, $a_{2z} = 0.92$, $t_c = 29.9999998$, $\Phi_c = 0.3004$, $D_L = 30,200$, $\iota = 0.80$, $\lambda = 3.50$, $\beta = 0.10$, $\psi = 1.50$.

The physical units for all parameters are listed in Table II.

1. Single-Signal Estimation and Analysis

We begin by analyzing each signal independently using full MCMC sampling to estimate the posterior distributions of the source parameters. Figure 6 shows the corner plots of one representative MBHB signal. The contours represent the 1σ and 2σ credible intervals of the marginalized posterior distributions. Results obtained with waveforms including higher-order modes are shown in red, while those using only the dominant (2,2) mode are shown in blue.

2. Two Wave Templates Matching Two-signals

Figure 7 shows the corner plots of MCMC results using two wave templates matching two-signals. The contours represent the 1σ and 2σ credible intervals of the marginalized posterior distributions. Results obtained with waveforms including higher-order modes are shown in red, while those using only the dominant (2,2) mode are shown in blue. These results demonstrate that incorporating higher-order modes can significantly reduce parameter uncertainties and help to break parameter degeneracies that arise in waveform modeling.

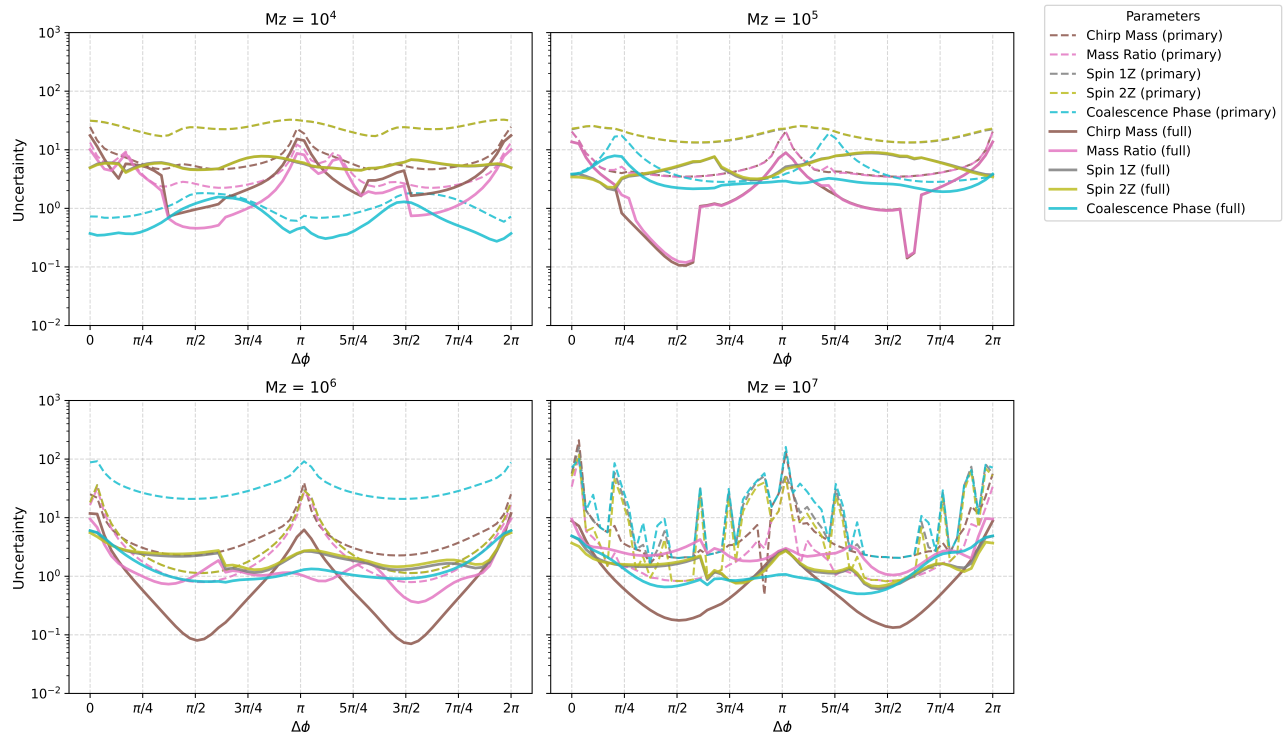


FIG. 5. Parameter uncertainty ratio $\rho - 1$ as a function of phase difference $\Delta\Phi = \Phi_1 - \Phi_2$, where Φ_1 and Φ_2 are the signal phases in the TDI-X2 channel. Only intrinsic parameters are shown. Dashed lines represent waveforms with the (2, 2) mode only; solid lines include higher-order modes. Here, $\Delta\mathcal{M}_z = 0$.

IV. CONCLUSIONS

In this study, we have systematically investigated the impact of source confusion on the parameter estimation of massive black hole binaries (MBHBs) in the context of space-based gravitational wave detection, specifically for the Taiji mission. While source confusion between MBHBs can occur, it is predominantly limited to overlaps between two signals. By incorporating realistic MBHB population models (PopIII, Q3d, and Q3nod) and simulating overlapping events in the time-frequency domain, we have quantified the effect of confusion using both the Fisher information matrix and full Bayesian inference via Markov Chain Monte Carlo (MCMC) techniques.

Our results demonstrate that when the detector-frame chirp mass difference between two signals is small ($\Delta\mathcal{M}_z/\mathcal{M}_z \lesssim 0.2\%$), parameter uncertainties can increase significantly, especially for high-mass systems. However, this degradation is notably mitigated when higher-order waveform modes are incorporated. Higher-order modes not only reduce overall parameter uncertainties but also help break degeneracies between intrinsic

parameters such as mass ratio and spin, particularly in cases of strong overlap.

We further show that even in the most challenging scenarios (e.g., $\Delta\mathcal{M}_z = 0$), the inclusion of higher-order modes limits the increase in uncertainty to within $\mathcal{O}(10^1)$ – $\mathcal{O}(10^2)$, highlighting their critical importance for accurate astrophysical inference. Our MCMC analysis confirms these trends and reveals that higher-order modes also improve the fidelity of joint parameter estimation for multiple overlapping sources.

These findings provide important guidance for future space-based gravitational wave missions. In particular, they underscore the necessity of using waveform templates that include higher-order modes in confusion-limited regimes and highlight the value of combining Fisher-based forecasting with full Bayesian inference for robust data analysis. As next-generation detectors aim to resolve increasingly complex source populations, understanding and mitigating the effects of source confusion will be essential for maximizing scientific return.

V. APPENDIXES

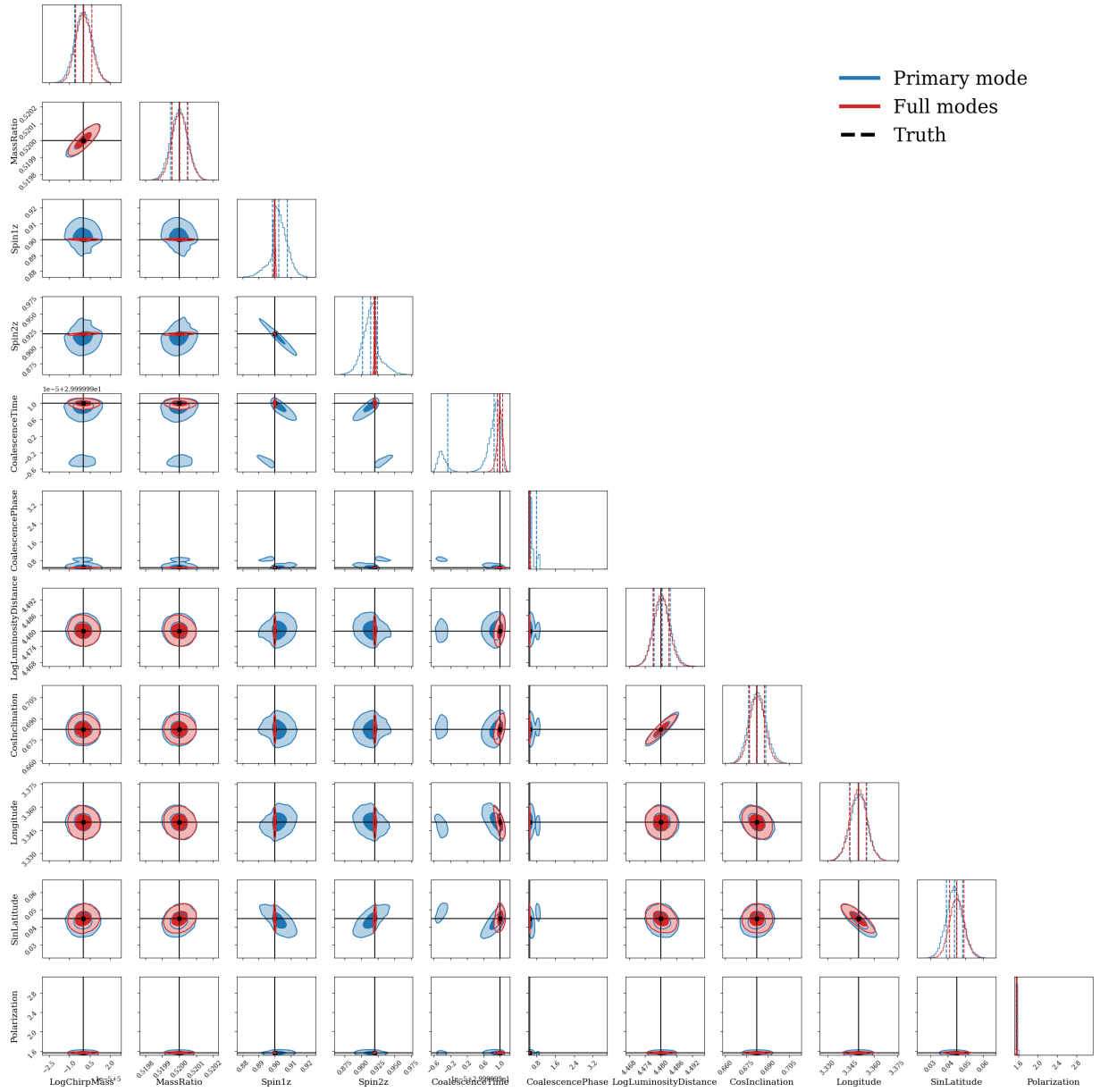


FIG. 6. Corner plot of the posterior distribution for a single MBHB signal using MCMC sampling. Red contours indicate results with higher-order modes; blue contours correspond to the dominant $(2, 2)$ mode only. The shaded regions represent the 1σ and 2σ credible intervals.

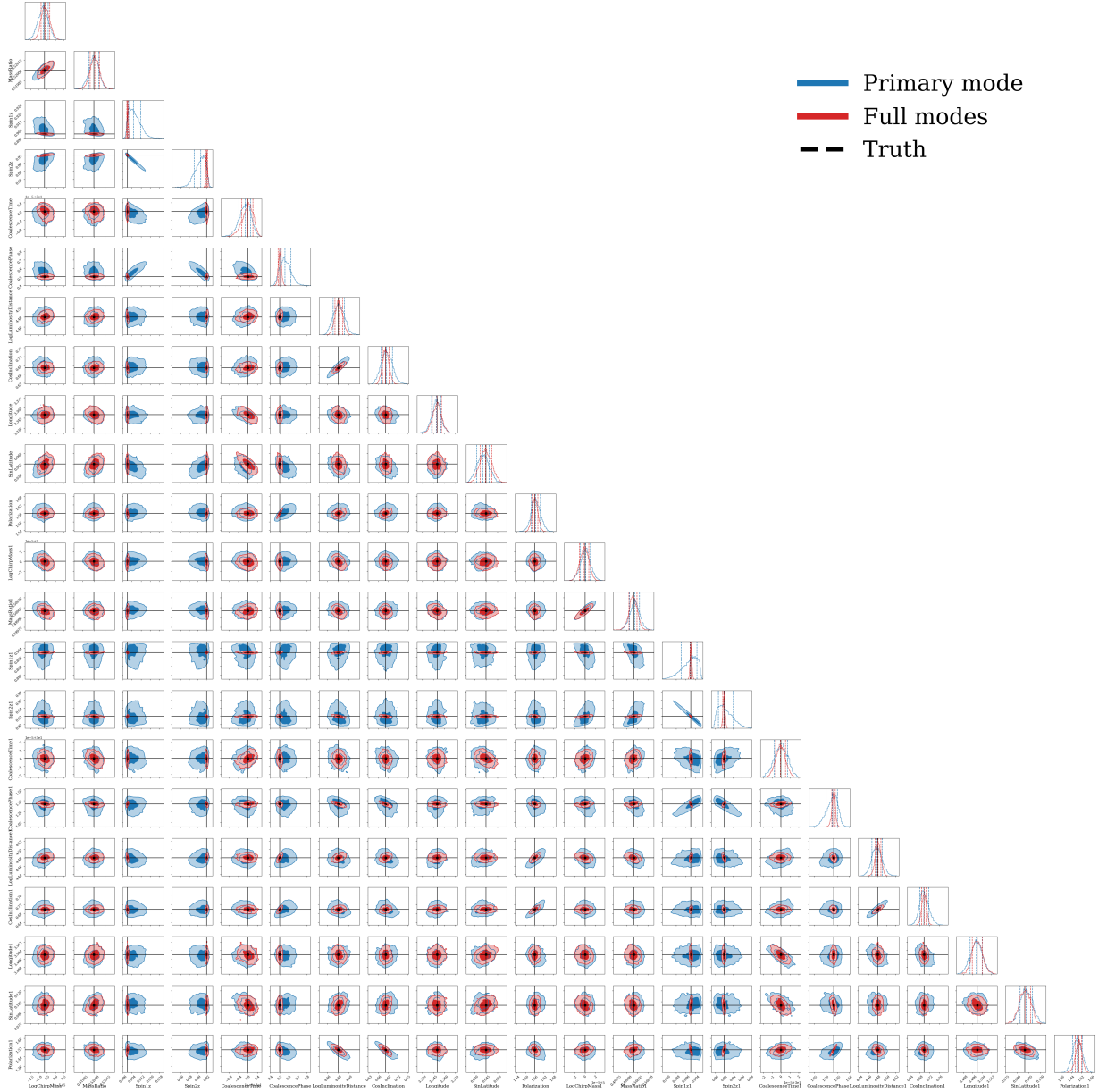


FIG. 7. Corner plot of the posterior distribution for two MBHB signals using MCMC sampling. Red contours indicate results with higher-order modes; blue contours correspond to the dominant (2, 2) mode only. The shaded regions represent the 1σ and 2σ credible intervals.

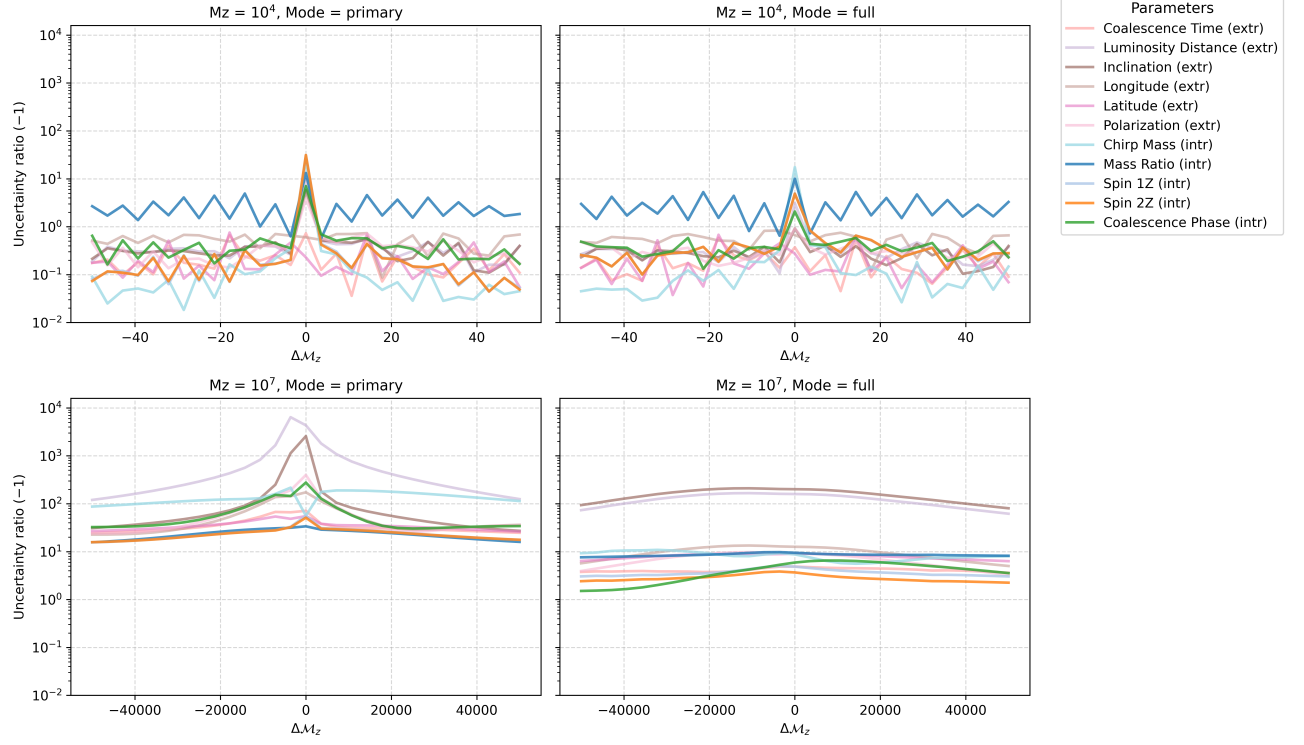


FIG. 8. Impact of chirp mass difference $\Delta\mathcal{M}_z$ on parameter uncertainty for two signals with $\mathcal{M}_z = 10^4$ and 10^7 , respectively. The left panels show results using only the dominant (2, 2) mode, while the right panels include higher-order modes. The x-axis spans 1% of the corresponding chirp mass.